ARCHIVE OF MECHANICAL ENGINEERING

DOI: 10.24425/ame.2025.157604 2026, Vol. 73, No. 1, pp. 19–41

Iman FARAJ [1], Jasim KHAWWAF[2]

Intelligent robust control of inverted pendulum using hierarchical sliding mode and ELM-based estimator

Received 27 June 2025, **Revised** 13 December 2025, **Accepted** 29 December 2025, **Published online** 20 January 2026

Keywords: inverted pendulum cart, hierarchical fast terminal sliding mode control, SIMO, underactuated system, ELM neural network

The Inverted Pendulum Cart (IPC) system is a significant challenge in control theory, is used as a benchmark for evaluating advanced actuator control techniques, and has critical applications in robotics and autonomous systems. This paper proposes a new control strategy based on a Hierarchical Non-Singular Fast Terminal Sliding Mode (HNFTSM) controller technique enhanced by an Extreme Learning Machine (ELM) neural network to achieve system stability. HNFTSM provides finite time convergence and resistance to disturbances and uncertainty, while the ELM contributes to estimating these disturbances to improve performance. The stability of this strategy is proven using the Lyapunov stability theory, which ensures that all system states reach the desired equilibrium in finite time. Furthermore, the proposed hierarchical control scheme guarantees finite-time convergence of all closed loop IPC states under bounded uncertainties. A comprehensive comparative analysis is conducted against other advanced control techniques, including HSMC, HNTSM, ELM-HNTSM, and conventional NFTSM controllers. Simulation results show that the proposed approach outperforms other methods in tracking accuracy, convergence speed, singularity avoidance, and chattering reduction, which enhances the effectiveness of system control and makes it promising for practical applications.

1. Introduction

The inverted pendulum-cart (IPC) system is one of the most classical benchmarks in control engineering due to its highly nonlinear dynamics, sensitivity to

✉ Iman FARAJ, email: imanattwan@alsafwa.edu.iq

[1]Department of Medical Instrumentation Engineering Techniques, Al-Safwa University, Karbala, Iraq

[2]Department of Electronic and Communication Engineering, Faculty of Engineering, University of Kufa, Najaf, Iraq

disturbances, and underactuated nature. These characteristics make the stabilization problem both theoretically rich and practically challenging [1–3]. Additional difficulties arise from sensor limitations, parameter uncertainties, and external unmodeled disturbances, which further complicate the control design [4]. As a SIMO underactuated system, the IPC lacks sufficient actuators relative to its degrees of freedom, making the development of reliable controllers an intricate task [5–7].

IPC-type dynamics appear in numerous real-world systems such as cranes, spacecraft, underwater vehicles, bipedal robots, manipulators, and rocket structures. Because of this widespread relevance, the IPC continues to serve as an ideal testbed for validating novel nonlinear and robust control methods [8, 9].

To simplify the stabilization problem, several studies have adopted linearization-based approaches that enable the use of conventional control tools [10, 11]. Comparative work in [12] evaluated PID, MPC, and LQR controllers, highlighting the ability of MPC to incorporate system constraints into an optimization framework. Meanwhile, [11] demonstrated how particle swarm optimization (PSO) can improve LQR performance by tuning gains efficiently under limited computational budgets. Related work in [13] further examined optimal stabilization strategies by analyzing the influence of sensor placement on system zeros to enhance robustness.

Although linear controllers can provide acceptable performance near nominal conditions, nonlinear effects and disturbances can quickly degrade their effectiveness. This motivates the use of intelligent and adaptive control techniques that can handle time-varying dynamics and uncertainties more effectively [14–16]. Sliding Mode Control (SMC), in particular, is widely recognized for its robustness against parameter variations and matched disturbances [17–20]. Enhanced variants such as ISMC and PID-SMC further improve transient behavior by modifying the sliding surface structure [21–23].

However, conventional SMC suffers from asymptotic convergence, which can lead to slow stabilization [24]. Terminal Sliding Mode Control (TSMC) addresses this limitation by ensuring finite-time convergence through nonlinear surface modification, but it may introduce singularity issues near the origin [25]. Fast Terminal Sliding Mode (FTSM) improves convergence speed but still fails to eliminate singularities [26]. To fully avoid singular behavior, nonsingular control approaches such as NTSM and NFTSM have been proposed, providing finite-time convergence across the entire state space [27–30].

Chattering, another common drawback of SMC-based methods, is often mitigated by using continuous approximations of the sign function, such as saturation functions, which improve practical applicability [31, 32]. Hybrid intelligent SMC approaches, including neural-network-based and fuzzy-based structures, have also shown strong performance under uncertainties [33].

Neural network methods are particularly effective when dealing with unknown or highly nonlinear dynamics. Among these, the Extreme Learning Machine (ELM)

stands out due to its simple structure, fast training, and ability to approximate nonlinear functions without iterative tuning [34, 35]. ELM has demonstrated strong capability in real-time estimation and compensation of dynamic uncertainties across various control applications [36, 37].

Given the SIMO nature of the IPC system, a hierarchical control architecture is an appropriate strategy to decouple and coordinate the dynamics of the pendulum and the cart. In this work, a hierarchical Nonsingular Fast Terminal Sliding Mode (HNFTSM) control framework is developed to ensure fast, finite-time convergence of both subsystems. Traditional SMC schemes typically require prior knowledge of disturbance bounds; however, this requirement is often impractical. To address this, the proposed method integrates an online ELM estimator capable of approximating the lumped uncertainty adaptively without needing predefined bounds.

The main contributions of this paper are summarized as follows:

1. A modified nonsingular terminal sliding manifold is proposed to accelerate convergence, especially for trajectories initially far from equilibrium.
2. A new sliding surface formulation is developed to guarantee the removal of singularities in the control law.
3. An adaptive ELM-based estimator is designed to approximate the lumped uncertainty in real time without requiring prior knowledge of disturbance bounds.
4. A hierarchical HNFTSM structure is formulated to exploit the SIMO characteristics of the IPC system, thereby improving coordination between pendulum and cart dynamics.
5. The proposed approach achieves enhanced robustness and improved tracking performance under varying uncertainties and disturbances, while ensuring finite-time convergence.

The remainder of this paper is organized as follows. Section 2 presents the IPC mathematical model and analyzes the uncertain dynamics. Section 3 details the proposed hierarchical control design and the integrated ELM estimator. Section 4 provides comparative simulation studies. Finally, Section 5 concludes the paper and outlines future extensions.

2. Mathematical modelling

This section presents the mathematical model of the inverted pendulum-cart (IPC) system, which forms the basis of the proposed control framework. The control objective is to regulate the pendulum angle θ and the cart position x by applying a horizontal control force u to the cart. The mechanical structure consists of a pendulum of mass m and length L, mounted on a cart of mass M. The cart moves along a frictionless horizontal track, as illustrated in Fig. 1. The physical parameters of the IPC system are summarized in Table 1.

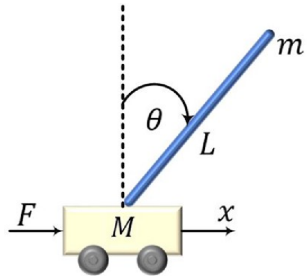

Fig. 1. Inverted pendulum-cart (IPC) model

Table 1. IPC physical parameters

Parameter	Symbol	Value	Unit
Pendulum mass	m	0.14	kg
Cart mass	M	1.00	kg
Pendulum length	L	0.125	m
Gravity acceleration	g	9.8	m/s^2

Following the formulation in [38], the nonlinear dynamics of the IPC system are written as:

$$\begin{cases} (M+m)\ddot{x} + mL\ddot{\theta}\cos\theta - mL\dot{\theta}^2\sin\theta = u + d, \\ mL\ddot{x}\cos\theta + mL^2\ddot{\theta} - mgL\sin\theta = 0, \end{cases} \tag{1}$$

where u is the control input and d is a bounded disturbance satisfying $|d(t)| \leqslant \Delta_d$.

To express these equations in state-space form, let's define the state vector as:

$$\mathbf{x} = \begin{bmatrix} x_1 \\ x_2 \\ x_3 \\ x_4 \end{bmatrix} = \begin{bmatrix} x \\ \dot{x} \\ \theta \\ \dot{\theta} \end{bmatrix}. \tag{2}$$

Using this notation, system (1) can be rewritten as:

$$\begin{cases} \dot{x}_1 = x_2, \\ \dot{x}_2 = f_1(x) + g_1(x)(u+d), \\ \dot{x}_3 = x_4, \\ \dot{x}_4 = f_2(x) + g_2(x)u, \end{cases} \tag{3}$$

where the nonlinear functions $f_1(x)$, $f_2(x)$ and the input gain functions $g_1(x)$, $g_2(x)$ are given by:

$$\begin{bmatrix} f_1(x) \\ f_2(x) \end{bmatrix} = \begin{bmatrix} M+m & mL\cos\theta \\ mL\cos\theta & mL^2 \end{bmatrix}^{-1} \begin{bmatrix} mL\dot{\theta}^2\sin\theta \\ mgL\sin\theta \end{bmatrix}. \tag{4}$$

$$\begin{bmatrix} g_1(x) \\ g_2(x) \end{bmatrix} = \begin{bmatrix} M+m & mL\cos\theta \\ mL\cos\theta & mL^2 \end{bmatrix}^{-1} \begin{bmatrix} 1 \\ 0 \end{bmatrix}. \tag{5}$$

From (4)-(5), the explicit subsystem dynamics become:

$$\ddot{x} = f_1(x) + g_1(x)(u+d), \tag{6}$$

$$\ddot{\theta} = f_2(x) + g_2(x)u. \tag{7}$$

To incorporate model uncertainties, (6) is rewritten as:

$$\ddot{x} = f_1(x) + \Delta f_1(x) + (g_1(x) + \Delta g_1(x))(u+d), \tag{8}$$

which can be expressed equivalently as:

$$\ddot{x} = f_1(x) + g_1(x)u + d_{\text{lump}}, \tag{9}$$

where the lumped uncertainty term is:

$$d_{\text{lump}} = \Delta f_1(x) + \Delta g_1(x)(u+d). \tag{10}$$

Here, $f_1(x), f_2(x)$ denote the nominal nonlinear dynamics, and $g_1(x), g_2(x)$ are the nominal input gain functions. The terms $\Delta f_1(x)$ and $\Delta g_1(x)$ represent bounded uncertainties arising from model inaccuracy, parameter variations, and unmodeled dynamics.

The 300% mass variation used in the uncertainty analysis is justified by two factors. First, recent IPC studies commonly test robustness using 100-200% parameter variations [39]. Second, the proposed controller is based on an HNFTSM sliding mode framework, which is inherently robust to large matched uncertainties. Thus, extending the variation to 300% provides a meaningful worst-case scenario that reflects the strong robustness properties of sliding mode control.

3. Control design

The proposed control framework consists of two main components. First, a robust hierarchical nonsingular fast terminal sliding mode (HNFTSM) controller is derived to guarantee accurate tracking and finite-time convergence of the pendulum and cart states. Second, an Extreme Learning Machine (ELM)-based estimator is employed to approximate the lumped uncertainties online, thereby improving the robustness of the closed-loop system.

The primary control objective is to ensure finite-time convergence of the system states to the sliding manifold, followed by asymptotic stability of the reduced-order dynamics on the sliding surface.

To meet this objective, a nonsingular fast terminal sliding mode controller is adopted [29]. A hierarchical sliding manifold is constructed based on nonlinear sliding surfaces, forming the foundation of the control design. The stability of the resulting control law is then established through Lyapunov theory.

3.1. Fundamental principles of Extreme Learning Machine (ELM)

Consider a set of N distinct training samples $(\mathbf{x}_i, \boldsymbol{\tau}_i)$, where $\mathbf{x}_i = [x_{i1}, x_{i2}, \cdots, \ldots x_{in}]^T \in \mathbb{R}^n$ and $\boldsymbol{\tau}_i = [\tau_{i1}, \tau_{i2}, \cdots, \tau_{im}]^T \in \mathbb{R}^m$. A standard single-layer feed-forward network (SLFN) with $\widetilde{N}$ hidden neurons is expressed as:

$$\sum_{i=1}^{\widetilde{N}} \beta_i G(\mathbf{x}_j, \boldsymbol{\gamma}_i, \alpha_i) = \tau_j, \quad j = 1, \cdots, N. \tag{11}$$

Here, $\boldsymbol{\gamma}_i = [\gamma_{i1}, \gamma_{i2}, \cdots, \gamma_{in}]^T$ represents the input weights, α_i is the hidden-layer bias, and $\beta_i = [\beta_{i1}, \cdots, \beta_{im}]^T$ is the output weight vector. The activation function is denoted by $G(\cdot)$.

Let $\mathbf{x} = [\mathbf{x}_1, \cdots, \mathbf{x}_N]$, $\boldsymbol{\gamma} = [\boldsymbol{\gamma}_1, \cdots, \boldsymbol{\gamma}_{\widetilde{N}}]$, and $\boldsymbol{\alpha} = [\alpha_1, \cdots, \alpha_{\widetilde{N}}]$. The SLFN then satisfies:

$$\mathbf{H}(\mathbf{x}, \boldsymbol{\gamma}, \boldsymbol{\alpha})\boldsymbol{\beta} = \mathbf{T}, \tag{12}$$

where the hidden-layer output matrix is:

$$\mathbf{H}(\mathbf{x}, \boldsymbol{\gamma}, \boldsymbol{\alpha}) = \begin{bmatrix} G(\mathbf{x}_1, \boldsymbol{\gamma}_1, \alpha_1) & \cdots & G(\mathbf{x}_1, \boldsymbol{\gamma}_{\widetilde{N}}, \alpha_{\widetilde{N}}) \\ \vdots & \ddots & \vdots \\ G(\mathbf{x}_N, \boldsymbol{\gamma}_1, \alpha_1) & \cdots & G(\mathbf{x}_N, \boldsymbol{\gamma}_{\widetilde{N}}, \alpha_{\widetilde{N}}) \end{bmatrix}. \tag{13}$$

The ELM trains much faster than traditional neural networks because its input weights are randomly assigned and only the output weights are computed analytically in one step. This avoids iterative backpropagation and local minima, making ELM suitable for real-time uncertainty estimation [35].

The least-squares solution of:

$$\|\mathbf{H}(\mathbf{x}, \boldsymbol{\gamma}, \boldsymbol{\alpha})\hat{\beta} - \mathbf{T}\| = \min_{\boldsymbol{\beta}} \|\mathbf{H}(\mathbf{x}, \boldsymbol{\gamma}, \boldsymbol{\alpha})\boldsymbol{\beta} - \mathbf{T}\| \tag{14}$$

is given by:

$$\hat{\beta} = \mathbf{H}^{\dagger}(\mathbf{x}, \boldsymbol{\gamma}, \boldsymbol{\alpha})\mathbf{T}, \tag{15}$$

where $\mathbf{H}^{\dagger}$ is the Moore-Penrose pseudo-inverse [40].

If the activation function is infinitely differentiable, then with probability one:

$$\|\mathbf{H}(\mathbf{x}, \boldsymbol{\gamma}, \boldsymbol{\alpha})\boldsymbol{\beta} - \mathbf{T}\| = \|\lambda(\mathbf{x})\| < \lambda_1, \tag{16}$$

where $\lambda(\mathbf{x})$ is the approximation error.

3.2. HNFTSM control strategy integrated with an ELM-based uncertainty estimator

The proposed control strategy combines an HNFTSM controller with an ELM-based estimator to achieve fast and robust tracking performance. The block diagram of the entire scheme is shown in Fig. 2.

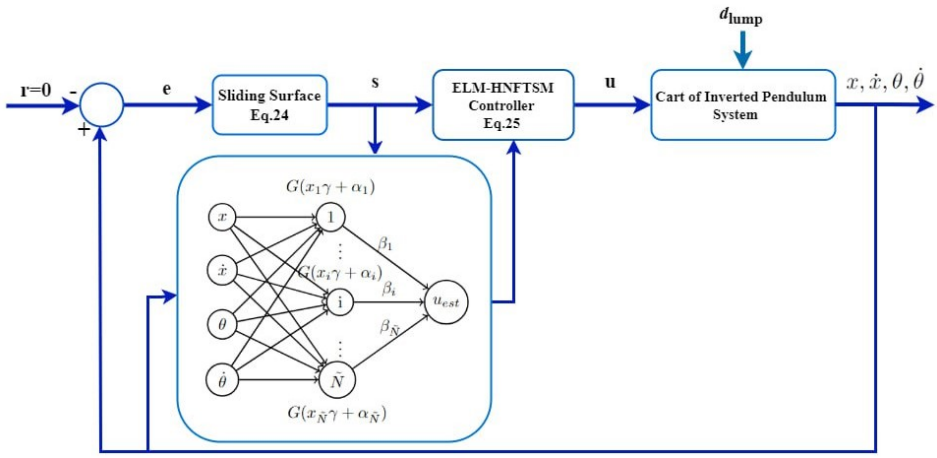

Fig. 2. Block diagram of the proposed control strategy

Define the tracking errors:

$$e_1 = x - x_d, \tag{17}$$

$$e_2 = \theta - \theta_d, \tag{18}$$

and their derivatives:

$$\dot{e}_1 = \dot{x} - \dot{x}_d, \tag{19}$$

$$\dot{e}_2 = \dot{\theta} - \dot{\theta}_d. \tag{20}$$

The second derivatives are:

$$\ddot{e}_1 = \ddot{x} - \ddot{x}_d, \tag{21}$$

$$\ddot{e}_2 = \ddot{\theta} - \ddot{\theta}_d. \tag{22}$$

The first-level sliding surfaces are defined by:

$$s_1 = e_1 + \delta_1 e_1^{[\Lambda_1]} + \sigma_1 \dot{e}_1^{[\zeta_1]}, \tag{23}$$

$$s_2 = e_2 + \delta_2 e_2^{[\Lambda_2]} + \sigma_2 \dot{e}_2^{[\zeta_2]}. \tag{24}$$

Here, δ_i and σ_i are positive constants, and ζ_i is an odd number satisfying:

$$1 < \zeta_i < 2, \qquad \Lambda_i > \zeta_i. \tag{25}$$

The second-level sliding surface is:

$$S = s_1 + \mu s_2, \tag{26}$$

with $\mu > 0$.

The control input is decomposed as:

$$u = u_1 + u_2, \tag{27}$$

where:

$$u_1 = u_{\text{eq1}} + u_{\text{sw1}} + u_{est}, \tag{28}$$

$$u_2 = u_{\text{eq2}} + u_{\text{sw2}}. \tag{29}$$

Differentiating the sliding surfaces yields:

$$\dot{S} = \dot{s}_1 + \mu \dot{s}_2. \tag{30}$$

$$\dot{s}_1 = \dot{e}_1 + \delta_1 \Lambda_1 |e_1|^{\Lambda_1 - 1} \dot{e}_1 + \sigma_1 \zeta_1 |\dot{e}_1|^{\zeta_1 - 1} (\ddot{x} - \ddot{x}_d). \tag{31}$$

$$\dot{s}_2 = \dot{e}_2 + \delta_2 \Lambda_2 |e_2|^{\Lambda_2 - 1} \dot{e}_2 + \sigma_2 \zeta_2 |\dot{e}_2|^{\zeta_2 - 1} (\ddot{\theta} - \ddot{\theta}_d). \tag{32}$$

By setting $\dot{s}_1 = 0$ and $\dot{s}_2 = 0$, the equivalent control signals become:

$$\begin{aligned} u_{\text{eq1}} &= \frac{1}{g_1(x)} \left(-\frac{1}{\sigma_1 \zeta_1} \left[\dot{e}_1^{[2-\zeta_1]} + \delta_1 \Lambda_1 |e_1|^{\Lambda_1 - 1} \dot{e}_1^{[2-\zeta_1]} \right] - f_1(x) + \ddot{x}_d \right), \\ u_{\text{eq2}} &= \frac{1}{g_2(x)} \left(-\frac{1}{\sigma_2 \zeta_2} \left[\dot{e}_2^{[2-\zeta_2]} + \delta_2 \Lambda_2 |e_2|^{\Lambda_2 - 1} \dot{e}_2^{[2-\zeta_2]} \right] - f_2(x) + \ddot{\theta}_d \right). \end{aligned} \tag{33}$$

The switching control inputs are:

$$\begin{aligned} u_{\text{sw1}} &= -\frac{k_1}{g_1(x)} \operatorname{sgn}(S), \\ u_{\text{sw2}} &= -\frac{k_2}{g_2(x)} \operatorname{sgn}(S), \end{aligned} \tag{34}$$

where k_i are positive gains.

The activation function of the ELM is chosen as:

$$G(\mathbf{x}, \boldsymbol{\gamma}, \alpha) = \frac{1}{1 + e^{-(\gamma x + \alpha)}}. \tag{35}$$

The lumped uncertainty is approximated by:

$$d_{\text{lump}} = \mathbf{H}(\mathbf{x}, \gamma, \alpha)\beta. \tag{36}$$

Although the lumped uncertainty d_{lump} contains the control input u, its boundedness is ensured by the HNFTSM control structure, since both the equivalent and switching terms remain bounded and the functions $g_1(x)$ $g_2(x)$ are bounded for all admissible states. Consequently, $u(t)$ and d_{lump} evolve within a bounded set, allowing the ELM to reliably approximate d_{lump} in real time.

Its estimated value is:

$$\hat{d}_{\text{lump}} = \frac{1}{g_1(x)}(\mathbf{H}\hat{\beta}). \tag{37}$$

Thus, the estimation-based compensation term is:

$$u_{est} = -\hat{d}_{\text{lump}}. \tag{38}$$

Define:

$$\psi_2 = \sigma_2\zeta_2\dot{e}_2^{(\zeta_2-1)}, \tag{39}$$

$$\psi_1 = \sigma_1\zeta_1\dot{e}_1^{(\zeta_1-1)}. \tag{40}$$

The ELM output weights are updated by:

$$\dot{\hat{\beta}}^T = \psi_1\eta|S|\mathbf{H}, \tag{41}$$

with adaptation gain $\eta > 0$ ensuring finite-time convergence.

During the sliding motion, the system trajectories converge to their desired references in finite time, thereby establishing the finite-time stability of the IPC system.

Proof: To examine the stability of the closed-loop system, consider the following Lyapunov candidate function:

$$V = \frac{1}{2}S^2 + \frac{1}{2\eta}\tilde{\beta}^T\tilde{\beta}, \tag{42}$$

where $\tilde{\beta} = \beta - \hat{\beta}$ is the estimation error of the ELM weights and $\eta > 0$ is the adaption gain.

The time derivative of V is computed as:

$$\dot{V} = S\dot{S} + \frac{1}{\eta}\tilde{\beta}^T\dot{\tilde{\beta}}. \tag{43}$$

From the definition of the hierarchical sliding variable:

$$\dot{S} = \dot{s}_1 + \mu\dot{s}_2, \tag{44}$$

we first evaluate $\dot{s}_1$ and $\dot{s}_2$.

Using Eqs.(2) and (31), the derivative $\dot{s}_1$ becomes:

$$\dot{s}_1 = \dot{e}_1 + \delta_1 \Lambda_1 e_1^{\Lambda_1 - 1} \dot{e}_1 + \sigma_1 \zeta_1 \dot{e}_1^{(\zeta_1 - 1)} \left[(f_1 + g_1 u_1 + d_{\text{lump}}) - \ddot{x}_d \right]. \tag{45}$$

Substituting the control law components from Eqs. (28), (33), (34), and (38), we obtain:

$$\begin{aligned} \dot{s}_1 &= \psi_1 \left(-k_1 \operatorname{sgn}(S) - \hat{d}_{\text{lump}} + d_{\text{lump}} \right) \\ &= \psi_1 \left(-k_1 \operatorname{sgn}(S) + \tilde{d}_{\text{lump}} \right) \\ &= \psi_1 \left(-k_1 \operatorname{sgn}(S) + \tilde{\beta} \mathbf{H} \right), \end{aligned} \tag{46}$$

where the lumped uncertainty estimation error is:

$$\begin{aligned} \tilde{d}_{\text{lump}} &= d_{\text{lump}} - \hat{d}_{\text{lump}} \\ &= \mathbf{H}\beta - \mathbf{H}\hat{\beta} \\ &= \mathbf{H}(\beta - \hat{\beta}) \\ &= \mathbf{H}\tilde{\beta}. \end{aligned} \tag{47}$$

Similarly, using Eqs. (7) and (32), $\dot{s}_2$ is given by:

$$\dot{s}_2 = \dot{e}_2 + \delta_2 \Lambda_2 e_2^{\Lambda_2 - 1} \dot{e}_2 + \sigma_2 \zeta_2 \dot{e}_2^{(\zeta_2 - 1)} \left[(f_2 + g_2 u_2) - \ddot{\theta}_d \right]. \tag{48}$$

Substituting Eq. (29), Eq. (33), and Eq. (34), we obtain:

$$\dot{s}_2 = -\psi_2 k_2 \operatorname{sgn}(S). \tag{49}$$

Now, substituting Eqs. (46) and (49) into Eq. (44), we obtain:

$$\dot{V} = \left[\psi_1 \left(-k_1 \operatorname{sgn}(S) + \tilde{\beta} \mathbf{H} \right) + \mu \left(-\psi_2 k_2 \operatorname{sgn}(S) \right) \right] S + \frac{1}{\eta} \tilde{\beta}^T \dot{\tilde{\beta}}. \tag{50}$$

Using the adaptation law from Eq. (41) and $\dot{\tilde{\beta}} = -\dot{\hat{\beta}}$, the expression becomes:

$$\begin{aligned} \dot{V} &= -(\psi_1 k_1 + \psi_2 k_2 \mu)|S| + \psi_1 |S| \, \tilde{\beta} \mathbf{H} - \frac{1}{\eta} \tilde{\beta}^T \psi_1 \eta |S| \mathbf{H} \\ &= -(\psi_1 k_1 + \psi_2 k_2 \mu)|S|. \end{aligned} \tag{51}$$

The ELM approximation error $\lambda(x)$ does not influence the closed-loop stability because the adaptive update law in (41) cancels the term $\tilde{\beta}^T \mathbf{H}$ in the Lyapunov derivative. Thus, $\dot{V}$ remains negative and is dominated by the terms $-\psi_1 k_1 |S|$ and $-\psi_2 k_2 \mu |S|$, ensuring finite-time convergence regardless of the approximation accuracy.

From Eqs. (39) and (40), since $\sigma_i > 0$ and $1 < \zeta_i < 2$, it follows that:

$$\psi_i > 0 \quad \text{for all } e_i \neq 0. \tag{52}$$

Thus, the Lyapunov derivative satisfies:

$$\dot{V} \leqslant 0 \qquad \text{since} \qquad \mu,\ k_i > 0, \tag{53}$$

which guarantees that the sliding variable S converges to zero in finite time.

Once the sliding surface is reached, the system trajectories evolve according to the reduced-order sliding dynamics, ensuring that both the cart position and pendulum angle tracking errors converge asymptotically to zero within a finite time, even under bounded uncertainties and external disturbances.

Remark 1: The hierarchical approach used for the NFTSM scheme will also be utilized for the NTSM and SMC approaches to assess the proposed controller. The ELM estimator will also be applied to both the HNFTSM and HNTSM methods. To provide a fair comparison, uniform parameter values are used in all methods, including the suggested controller, as presented in Table 2. The controller parameters were selected following the guidelines reported in [30], ensuring consistency with previously validated NFTSM based designs."

Table 2. Control parameters used for HNFTSM, HSMC, and HNTSM methods

Parameter	Value	Parameter	Value
ζ_1	1.05	ζ_2	1.15
σ_1	6	σ_2	1.8
δ_1	10	δ_2	7
Λ_1	10	Λ_2	2
k_1	10	k_2	10
c_1	4	c_2	1.5
μ	1		

Remark 2: The presence of chattering in the control signal is due to the signum function in Eq. (34), which could have a detrimental impact on the performance of the system. To reduce this chattering, it is customary to substitute the signum function with a saturation function. This strategy is used in all the previously described methods.

4. Results and discussion

This section demonstrates the efficiency of the proposed ELM-HNFTSM controller for the inverted pendulum. Four different scenarios were examined and compared to the HSMC, HNTSM, ELM-HNTSM, and HNFTSM controllers to assess the ELM-HNFTSM 's performance in terms of robustness, respond quickly, its ability to estimate uncertainties, and maintaining accuracy. The first scenario

evaluated performance under normal circumstances. The second scenario assessed the resistance to parameter changes, while the third scenario tested the performance under the impact of an external disturbance. The RMS values of all controllers were analyzed under all three scenarios (nominal, uncertainty, and disturbance) using the following equation:

$$\mathrm{RMS}(e) = \sqrt{\sum_{i=1}^{t} \frac{e_i^2}{t}} \tag{54}$$

Here, t is the sample number. In all simulations, the pendulum is started with an angular position of -0.05 rad.

The adopted ELM selects node numbers $\tilde{N}$ and adaptive gain η as 20 and 70, respectively. The starting parameters (γ, α) are randomly selected from the intervals $[-1, 1]$ and $[0, 1]$, respectively.
Then, a sliding mode SMC surface is defined as:

$$s_i = \dot{e}_i + c_i e_i, \quad c_i > 0 \tag{55}$$

And the NTSM sliding surface is defined as:

$$s_i = e_i + \sigma_i \dot{e}_i^{\zeta_i} \quad 1 < \zeta_i < 2 \quad \text{and} \quad \sigma_i > 0 \tag{56}$$

4.1. Angular position response and stabilization

The comparative analysis of the control methods HSMC, HNTSM, ELM-HNTSM, HNFTSM, and the proposed method is shown in Figs. 3–5, with distinguished differences in robustness, accuracy, and convergence speed. The HSMC method exhibits more significant oscillations and slower convergence, indicating less robustness under the tested conditions. In contrast, HNTSM and HNFTSM methods demonstrate improved stability and faster convergence, although they still experience minor oscillations. The HNTSM and HNFTSM methods exhibit a high initial peak in the angular response due to the complex differential equations governing them, making them more sensitive to initial conditions such as angular velocity and tilt angle. This sensitivity often results in an initial overshoot, as these methods are designed to quickly reduce the error. Consequently, introducing the ELM estimator into ELM-HNTSM and the proposed method further refines these results, yielding smoother trajectories with faster stabilization. This indicates that the ELM estimator effectively enhances the control strategies, improving both robustness and convergence speed and reducing the RMS error from (0.013,0.014) to (0.0035,0.006) for the angular tracking errors of HNFTSM and HNTSM, respectively, as noticed in Table 3.

Fig. 4 demonstrates that the proposed control strategy maintains stronger robustness than the other compared methods. Incorporating the ELM estimator further improves the behavior of both HNTSM and HNFTSM methods, as reflected

by the low RMS values of the position tracking error (ELM-HNTSM: 0.0070 and ELM-HNFTSM: 0.0030).

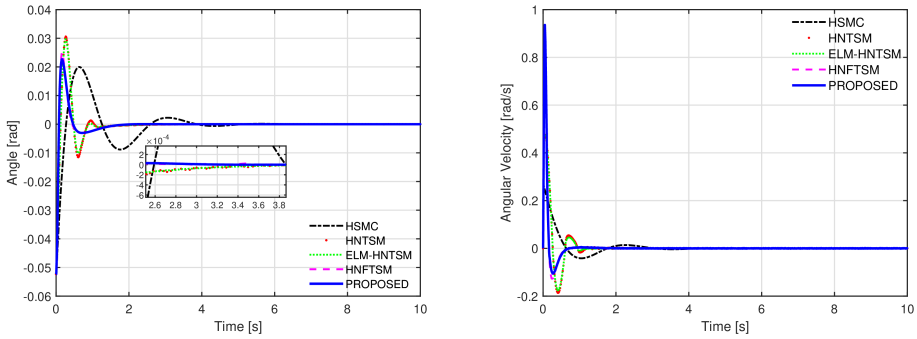

(a) Angular position (b) Angular velocity

Fig. 3. (a) Angular position and (b) angular velocity of the pendulum under nominal conditions

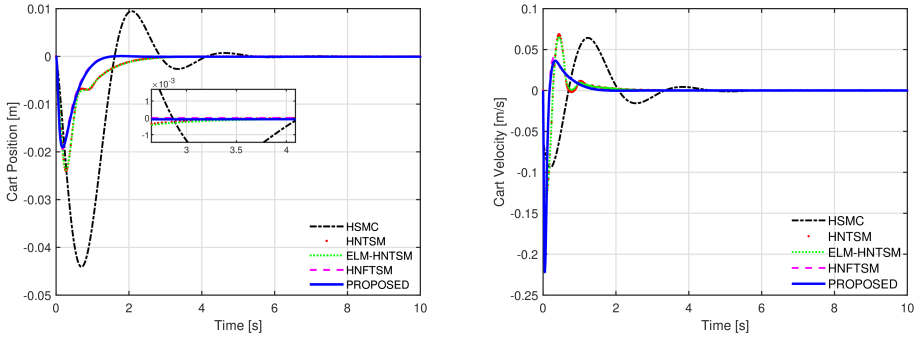

(a) Cart position (b) Cart velocity

Fig. 4. (a) Cart position and (b) cart velocity under nominal conditions

The control signal shown in Fig. 5b offers valuable information about robustness, suppression of chattering, passage around singularities, and precision. The proposed scheme provides a stable control signal with suppressed chattering and ensures proper performance without encountering any singularity. The peak initial control input in the proposed scheme represents a proactive approach to quickly move the cart of the inverted pendulum system towards a balanced position. This proactive control input helps in quickly responding to the system, which in turn promotes it towards achieving stability. The scheme reduces chattering effectively and provides a smooth control input, which plays a vital role in acquiring precise control performance of different techniques on the sliding surface (S). Regarding settling time, the proposed method exhibits the fastest and most stable response, outperforming other methods. The HNFSM (red) method shows a slightly delayed

but stable response, whereas the HSMC (black) method demonstrates a slower response with more initial oscillation. Adding the ELM estimator to the HNFTSM and HNTSM methods improves robustness against uncertainties and disturbances. This leads to a more accurate and stable sliding surface trajectory, particularly in the proposed method.

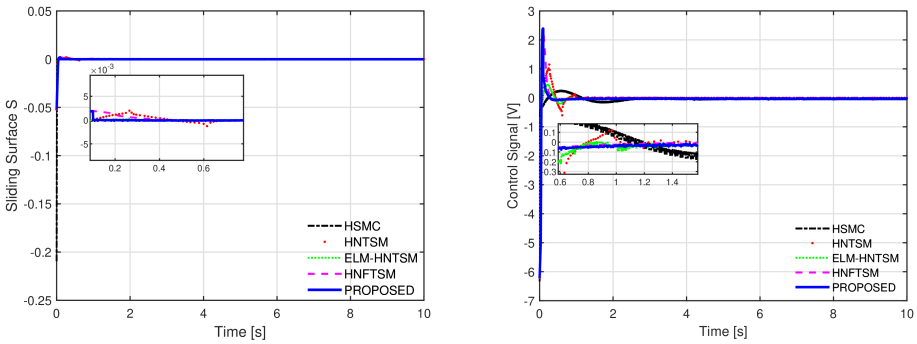

(a) Sliding surface (b) Control signal

Fig. 5. (a) Sliding surface and (b) control signal under nominal conditions

Table 3. Comparison of RMS for position and angular tracking errors for five stabilizing controllers

Controller	Scenario	Position RMS error	Angular RMS error
HSMC	Nominal	0.0120	0.0171
	Uncertainty	0.0121	0.0171
	Shock Disturbance	0.0146	0.0182
	Periodic Disturbance	0.0124	0.0169
HNTSM	Nominal	0.0075	0.0140
	Uncertainty	0.0087	0.0141
	Shock Disturbance	0.0080	0.0161
	Periodic Disturbance	0.0070	0.0129
ELM-HNTSM	Nominal	0.0070	0.0060
	Uncertainty	0.0075	0.0090
	Shock Disturbance	0.0069	0.0060
	Periodic Disturbance	0.0060	0.0066
HNFTSM	Nominal	0.0050	0.0130
	Uncertainty	0.0051	0.0129
	Shock Disturbance	0.0060	0.0140
	Periodic Disturbance	0.0052	0.0120
Proposed ELM-HNFTSM	Nominal	0.0030	0.0035
	Uncertainty	0.0040	0.0041
	Shock Disturbance	0.0036	0.0030
	Periodic Disturbance	0.0037	0.0035

4.2. Parameter variations and system robustness

The second simulated study analyzes the controllers' changes in parameter changes. When the cart and pendulum Weights are increased by 300% (m = 0.42 kg M = 3 kg), Figs. 6, 7, 8 show that while mass of the pendulum and cart increase, it will not have a great effect on the control strategies for balancing IPC system. From Table 3, we can conclude by the RMS errors that these methods are robust to system dynamics variations. However, the control input signals exhibit significant variations at the start of the execution due to the initial high force requirement to compensate for the increased weight. The proposed method outperforms others in speed, robustness, accuracy, chattering reduction, and singularity avoidance.

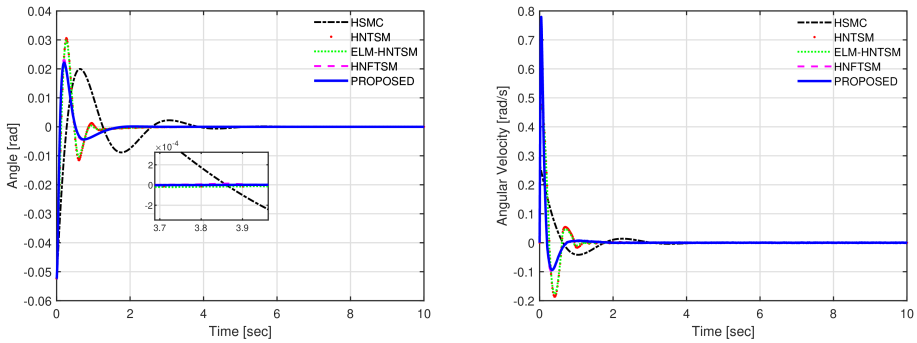

(a) Angular position (b) Angular velocity

Fig. 6. (a) Angular position and (b) angular velocity responses under uncertainty conditions (with 300% increase in cart and pendulum masses)

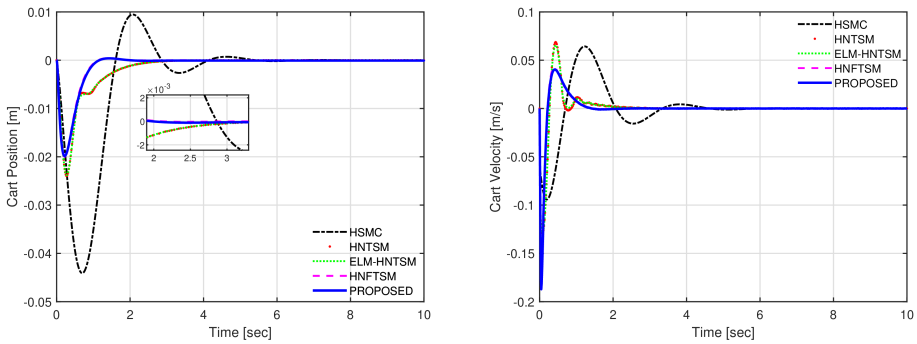

(a) Cart position (b) Cart velocity

Fig. 7. (a) Cart position and (b) cart velocity responses under uncertainty conditions (with 300% increase in cart and pendulum masses)

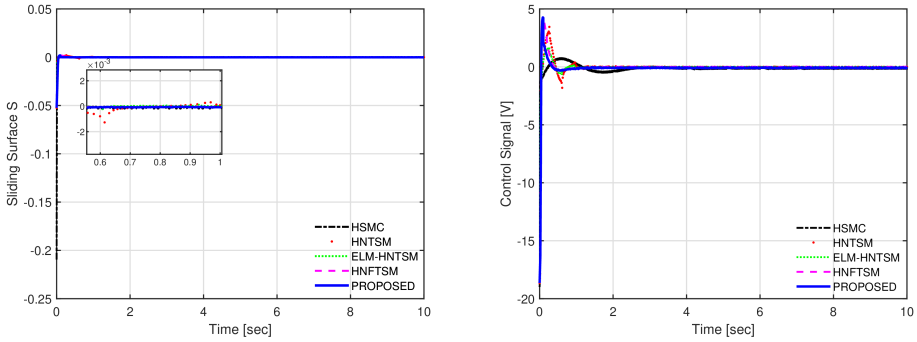

(a) Sliding surface (b) Control signal

Fig. 8. (a) Sliding surface and (b) control signal responses under uncertainty conditions (with 300% increase in cart and pendulum masses)

4.3. Handling and rejection of disruptions

The third simulation evaluated the controllers' ability to handle external disturbances by subjecting the IPC to both shock and periodic disturbances. Initially, the system was exposed to a shock disturbance of magnitude 7 for a duration of 1 second, starting at the 5th second. The results demonstrated the following key findings:

The proposed NFTSM method combined with the ELM estimator is the most effective approach for counteracting external disturbances, as evidenced by its superior performance in Figs. 9, 10, 11. This method shows the fastest response in facing disturbances, with a quick return to the desired state, outperforming the other methods, including HSMC, HNTSM, and HNFTSM. Integrating the ELM estimator is crucial, as it significantly enhances the control system's disturbance rejection capability, minimizing the external shock's effect.

Regarding the pendulum's angle and angular velocity, the proposed method exhibits the least deviation and the fastest stabilization, as reflected by the lower RMS error values of 0.0036 for the cart position and 0.003 for the angular tracking error listed in Table 3, effectively countering the shock disturbance. Based on the RMS measure, these low error values indicate that the proposed controller achieves a faster decay of residual oscillations under shock disturbance. This behavior is attributed to the rapid attenuation of post-disturbance transients, which significantly reduces the accumulated error energy over the evaluation interval used for RMS computation. Consequently, the angular velocity stabilizes faster, ensuring that the pendulum returns to its upright position with minimal oscillations.

The proposed method again excels for the cart's position and velocity in Fig. 10a, showing the smallest position deviation and quickest return to the desired position, demonstrating its effectiveness in maintaining the cart's stability.

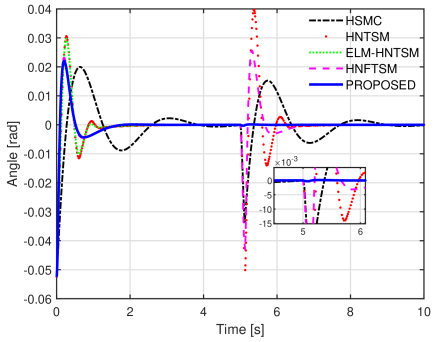

(a) Angular position

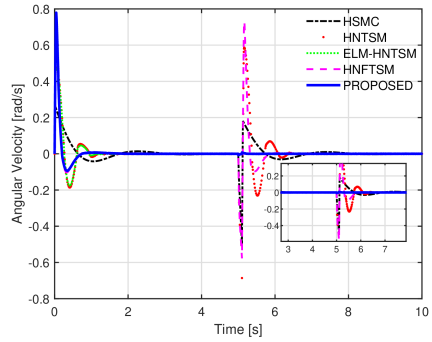

(b) Angular velocity

Fig. 9. (a) Angular position and (b) angular velocity responses under shock disturbance

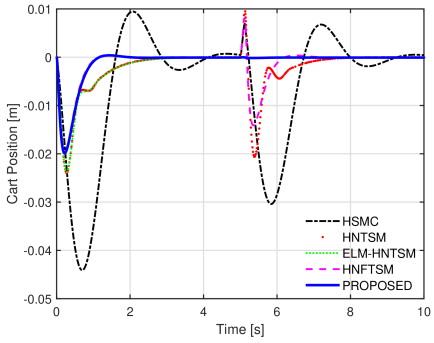

(a) Cart position

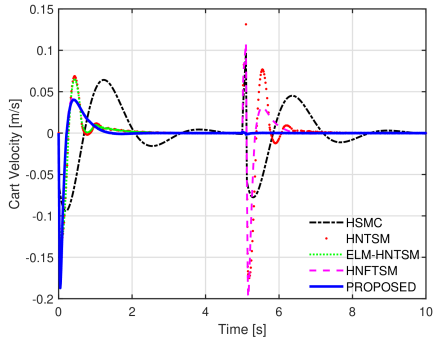

(b) Cart velocity

Fig. 10. (a) Cart position and (b) cart velocity responses under shock disturbance

It can be seen in Fig. 11 for the sliding surface and a control signal that the HSMC demonstrates a slower response with noticeable chattering faces, singularity issues, and less stability, recovering eventually but with less robustness. HNTSM shows improved disturbance rejection speed but still exhibits significant chattering, indicating sensitivity to disturbances. ELM-HNTSM benefits from the ELM estimator, reducing chattering and improving speed, yet some oscillations remain in the control signal. HNFTSM significantly reduces chattering and shows faster and smoother disturbance rejection.

The proposed ELM-NFTSM, however, offers the best performance, with the fastest recovery, minimal chattering, and smooth control signals, effectively avoiding singularity problems and neglecting the disturbance. In conclusion, the proposed ELM-NFTSM stands out as the most effective method, providing superior robustness and optimal control for the system.

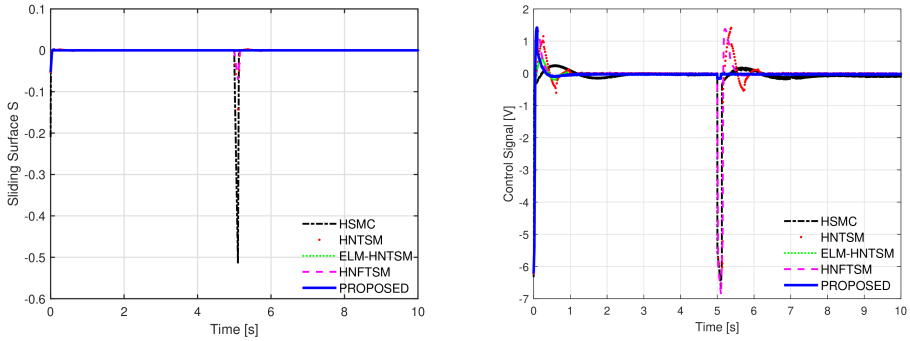

(a) Sliding surface (b) Control signal

Fig. 11. (a) Sliding surface and (b) control signal responses under shock disturbance

Fig. 12a demonstrates the effectiveness of the ELM estimator in tracking the external disturbance, as indicated by the close alignment of the estimated disturbance (blue) with the actual disturbance (red).

Fig. 12b shows the error between the actual disturbance and the ELM estimator's prediction, which remains minimal except for a brief spike during the disturbance. This small error indicates the estimator's strong performance in accurately modelling the disturbance.

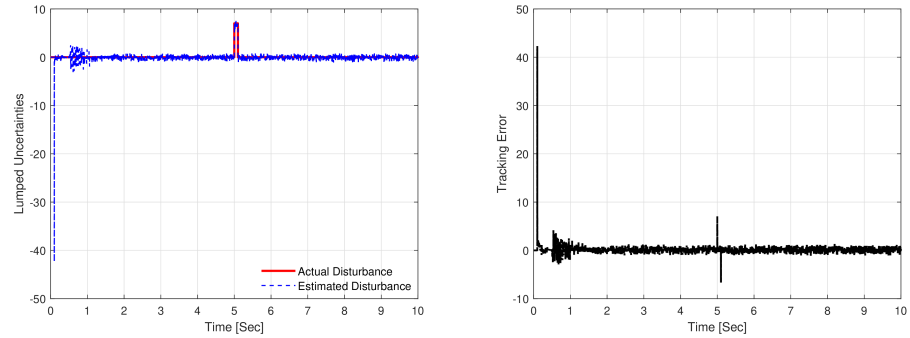

(a) Lumped uncertainties (b) Error tracking of ELM

Fig. 12. Responses under shock disturbance: (a) Lumped uncertainties and (b) ELM error tracking

After that, the system was subjected to a periodic disturbance (d(t)=sin(t)) for 10 seconds; the responses were captured in Figs. 13–14, showing the angle, angular velocity, cart position, and cart velocity, respectively. The results highlight the robustness of the control methods in handling disturbances, with the proposed method demonstrating the most effective periodic disturbance rejection, as reflected in the lower RMS error values presented in Table 3.

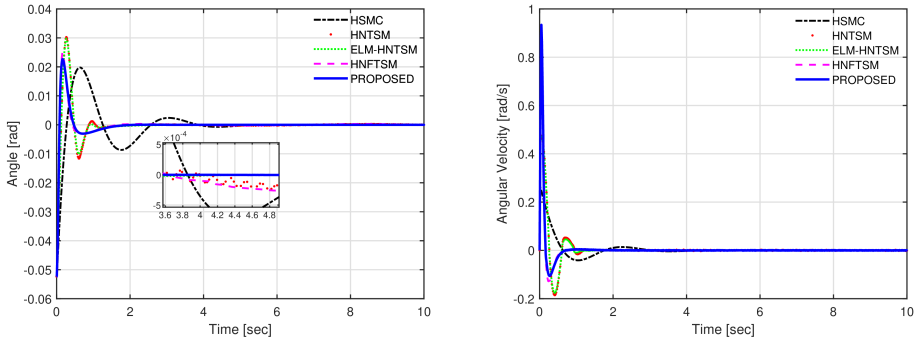

(a) Angular position (b) Angular velocity

Fig. 13. Responses under periodic signal: Pendulum angular position and velocity

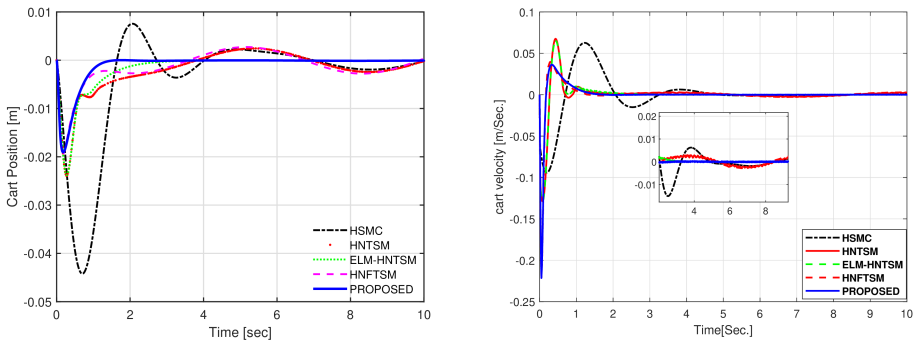

(a) Cart position (b) Cart velocity

Fig. 14. Responses under periodic signal: Cart position and velocity

The control signal shown in Fig.15b indicates reduced chatter and strong stability, particularly for the proposed method with the ELM estimator, which effectively reduces the impact of disturbances.

The integration of ELM with HNTSM, along with proposed control strategies, greatly enhances the precision of disturbance estimation, as shown in Fig. 16a, where it can be visualized that the estimated disturbances match with actual disturbances, demonstrating the estimator's effectiveness in capturing dynamic variations and improving overall system performance. Fig. 16b further supports this, showing minimal error between the estimated and actual disturbances, confirming the effectiveness of the ELM estimator in enhancing system performance.

The initial spike in Fig.16b, Fig.12a, the neural network tracking turbulence, can be attributed to the fact that the ELM network relies on randomly generating hidden layer weights. This random initialization leads to temporary instability at

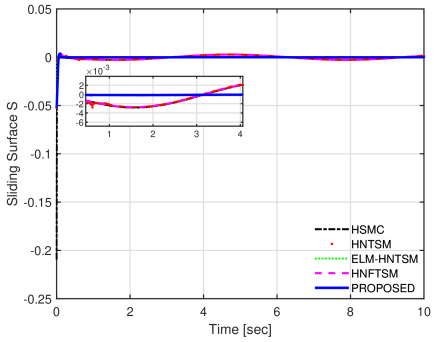

(a) Sliding surface

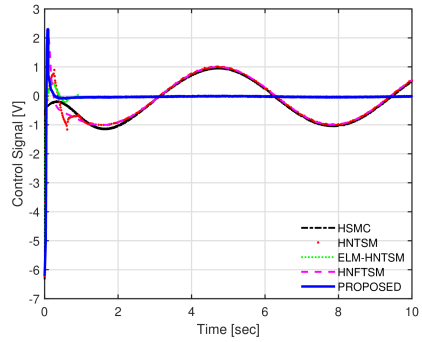

(b) Control signal

Fig. 15. Responses under periodic signal

the start of the model run. However, the network quickly stabilizes its estimates over time and approximates the disturbance well.

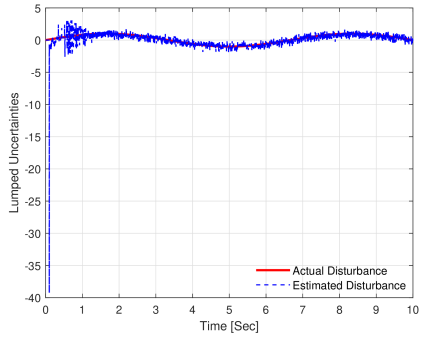

(a) Lumped uncertainties

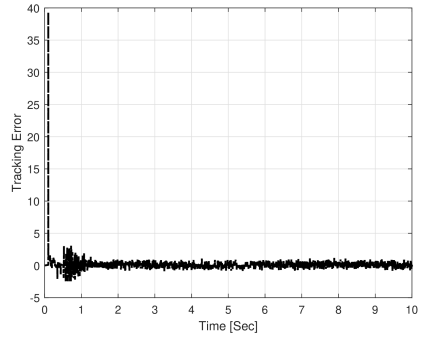

(b) Error tracking of ELM

Fig. 16. Responses under periodic disturbance: Lumped uncertainties and error tracking

5. Conclusions

This paper presents a new ELM-HNFTSM control strategy for stabilizing the IPC system modelled as a SIMO system. The proposed method ensures simultaneous control of the cart and pendulum subsystems by employing a hierarchical control structure, achieving rapid error convergence and robust disturbance rejection. Integrating the ELM neural network into the HNFTSM framework further enhances the system's adaptability to uncertainties and external disturbances, improving control performance. Comparative simulations confirm the superiority of the proposed method over existing approaches, particularly in terms of tracking accuracy, convergence speed, and chattering reduction. Overall, the proposed NFTSM

with ELM is the most robust and fastest method of handling (normal, uncertainties and external disturbance) conditions, making it the best choice for controlling the IPC system with such conditions.

References

[1] H.D. Le and T. Nestorović. A novel hierarchical recursive nonsingular terminal sliding mode control for inverted pendulum. *Actuators*, 12(12):462, 2023. doi: 10.3390/act12120462.

[2] Y. Yang and Y. Li. Design of virtual simulation experiment teaching project of linear inverted pendulum control system. In *Proc. 36th Youth Academic Annual Conference of Chinese Association of Automation (YAC)*, pages 93–97. IEEE, 2021. doi: 10.1109/YAC53711.2021.9486608.

[3] Iman Faraj and Jasim Khawwaf. Efficient fast nonsingular terminal sliding mode control to balance inverted pendulum system. In *AIP Conference Proceedings*, volume 3318, page 060002. AIP Publishing LLC, 2025. doi: 10.1063/5.0286159.

[4] Vo Nhu Thanh, Pham Anh-Duc, and Nguyen Dac Minh Triet. Hierarchical sliding mode control with oscillation compensation for low-cost inverted pendulum systems using hardware-in-loop. *Archive of Mechanical Engineering*, 72(1):31–55, 2025. doi: 10.24425/ame.2025.153737.

[5] D. Gontijo, J. M. Araújo, L. Frezzato, and F. de Oliveira Souza. Dynamic output feedback of second-order systems: An observer-based controller with linear matrix inequality design. *Actuators*, 13(6):216, 2024. doi: 10.3390/act13060216.

[6] Y. Kim and S. Kwon. Robust stabilization of underactuated two-wheeled balancing vehicles on uncertain terrains with nonlinear-model-based disturbance compensation. *Actuators*, 11(11):339, 2022. doi: 10.3390/act11110339.

[7] V.D. Ha, H.X. Dung, N.M. Tam, and N.V.D. Hai. Hierarchical fuzzy sliding mode control for a class of SIMO under-actuated systems. *Journal of Technical Education Science*, 12(Special Issue 02):83–91, 2017.

[8] H. Gao, S. Wang, K. Shan, C. Mu, X. Wang, B. Su, and H. Yu. Stable rapid sagittal walking control for bipedal robot using passive tendon. *Actuators*, 13(7):240, 2024. doi: 10.3390/act13070240.

[9] S. Kajita, M. Morisawa, K. Miura, S. Nakaoka, K. Harada, K. Kaneko, F. Kanehiro, and K. Yokoi. Biped walking stabilization based on linear inverted pendulum tracking. In *2010 IEEE/RSJ International Conference on Intelligent Robots and Systems*, pages 4489–4496. IEEE, 2010. doi: 10.1109/IROS.2010.5651082.

[10] M.S. Mahmoud and M.T. Nasir. Robust control design of wheeled inverted pendulum assistant robot. *IEEE/CAA Journal of Automatica Sinica*, 4(4):628–638, 2017. doi: 10.1109/JAS.2017.7510613.

[11] S. Howimanporn, S. Thanok, S. Chookaew, and W. Sootkaneung. Design and implementation of PSO based LQR control for inverted pendulum through PLC. In *2016 IEEE/SICE International Symposium on System Integration (SII)*, pages 664–669. IEEE, 2016. doi: 10.1109/SII.2016.7844075.

[12] P. Bakaráč, M. Klaučo, and M. Fikar. Comparison of inverted pendulum stabilization with PID, LQ, and MPC control. In *2018 Cybernetics and Informatics (K&I)*, pages 1–6. IEEE, 2018. doi: 10.1109/CYBERI.2018.8337540.

[13] C. Chen, D. Zhao, and L. Qiu. Control of an under-sensed and under-actuated linear inverted pendulum. In *2018 57th Annual Conference of the Society of Instrument and Control Engineers of Japan (SICE)*, pages 1301–1306. IEEE, 2018. doi: 10.23919/SICE.2018.8492573.

[14] A. Al-Mahturi, F. Santoso, M.A. Garratt, and S.G. Anavatti. An intelligent control of an inverted pendulum based on an adaptive interval type-2 fuzzy inference system. In *2019 IEEE International Conference on Fuzzy Systems (FUZZ-IEEE)*, pages 1–6. IEEE, 2019. doi: 10.1109/FUZZ-IEEE.2019.8858948.

[15] S. Zeghlache, M. Z. Ghellab, A. Djerioui, B. Bouderah, and M. F. Benkhoris. Adaptive fuzzy fast terminal sliding mode control for inverted pendulum-cart system with actuator faults. *Mathematics and Computers in Simulation*, 210:207–234, 2023. doi: 10.1016/j.matcom.2023.03.005.

[16] Z. Ping, M. Zhou, C. Liu, Y. Huang, M. Yu, and J.-G. Lu. An improved neural network tracking control strategy for linear motor-driven inverted pendulum on a cart and experimental study. *Neural Computing and Applications*, pages 1–8, 2022. doi: 10.1007/s00521-021-05986-9.

[17] Q. Wu, X. Wang, L. Hua, and M. Xia. Modeling and nonlinear sliding mode controls of double pendulum cranes considering distributed mass beams, varying roped length and external disturbances. *Mechanical Systems and Signal Processing*, 158:107756, 2021. doi: 10.1016/j.ymssp.2021.107756.

[18] S. Irfan, A. Mehmood, M. T. Razzaq, and J. Iqbal. Advanced sliding mode control techniques for Inverted Pendulum: Modelling and simulation. *Engineering Science and Technology, an International Journal*, 21(4):753–759, 2018. doi: 10.1016/j.jestch.2018.06.010.

[19] T. Al-Hsnawy and A. Al-Ghanimi. A review of control methods for quadrotor UAV. *Kufa Journal of Engineering*, 15(4):98–124, 2024. doi: 10.30572/2018/KJE/150408.

[20] F.F.M. El-Sousy, K. A. Alattas, O. Mofid, S. Mobayen, and A. Fekih. Robust adaptive super-twisting sliding mode stability control of underactuated rotational inverted pendulum with experimental validation. *IEEE Access*, 10:100857–100866, 2022. doi: 10.1109/ACCESS.2022.3208412.

[21] G.P. Incremona, A. Ferrara, and L. Magni. MPC for robot manipulators with integral sliding modes generation. *IEEE/ASME Transactions on Mechatronics*, 22(3):1299–1307, 2017. doi: 10.1109/TMECH.2017.2674701.

[22] M. Ming, W. Liang, Z. Feng, J. Ling, A. Mamun, and X. Xiao. PID-type sliding mode-based adaptive motion control of a 2-DOF piezoelectric ultrasonic motor driven stage. *Mechatronics*, 76:102543, 2021. doi: 10.1016/j.mechatronics.2021.102543.

[23] M. Van, S.S. Ge, and H. Ren. Robust fault-tolerant control for a class of second-order nonlinear systems using an adaptive third-order sliding mode control. *IEEE Transactions on Systems, Man, and Cybernetics: Systems*, 47(2):221–228, 2016. doi: 10.1109/TSMC.2016.2557220.

[24] G. Chen, Y. Song, and Y. Guan. Terminal sliding mode-based consensus tracking control for networked uncertain mechanical systems on digraphs. *IEEE Transactions on Neural Networks and Learning Systems*, 29(3):749–756, 2016. doi: 10.1109/TNNLS.2016.2636323.

[25] H. Wang, Z. Man, H. Kong, Y. Zhao, M. Yu, Z. Cao, J. Zheng, and M. T. Do. Design and implementation of adaptive terminal sliding-mode control on a steer-by-wire equipped road vehicle. *IEEE Transactions on Industrial Electronics*, 63(9):5774–5785, 2016. doi: 10.1109/TIE.2016.2573239.

[26] X. Yu and Z. Man. Fast terminal sliding-mode control design for nonlinear dynamical systems. *IEEE Transactions on Circuits and Systems I: Fundamental Theory and Applications*, 49(2):261–264, 2002. doi: 10.1109/81.983876.

[27] J. Khawwaf, J. Zheng, R. Lu, A. Al-Ghanimi, and B. I. Kazem. Robust tracking control of an IPMC actuator using nonsingular terminal sliding mode. *Smart Materials and Structures*, 26(9):095042, 2017. doi: 10.1088/1361-665X/aa7d69.

[28] E. Zhong, S. Wang, C. Zhai, and W. Li. Improved non-singular fast terminal sliding mode control with hysteresis compensation for piezo-driven fast steering mirrors. *Actuators*, 14(4):170, 2025. doi: 10.3390/act14040170.

[29] L. Yang and J. Yang. Nonsingular fast terminal sliding-mode control for nonlinear dynamical systems. *International Journal of Robust and Nonlinear Control*, 21(16):1865–1879, 2011. doi: 10.1002/rnc.1666.

[30] I. Faraj and J. Khawwaf. Efficient combined non-singular fast terminal sliding mode control for robust balancing of inverted pendulum cart. *International Journal of Advanced Mechatronic Systems*, 12(2):93–105, 2025. doi: 10.1504/IJAMECHS.2025.145730.

[31] S. Wang, D. Wang, A. Ma, X. Yan, and S. Zhao. Intelligent robust control of roadheader based on disturbance observer. *Actuators*, 14(1):36, 2025. doi: 10.3390/act14010036.

[32] H. Li, L. Dou, and Z. Su. Adaptive nonsingular fast terminal sliding mode control for the electromechanical actuator. *International Journal of Systems Science*, 44(3):401–415, 2013. doi: 10.1080/00207721.2011.601348.

[33] S. Irfan, L. Zhao, S. Ullah, A. Mehmood, and M.F.U. Butt. Control strategies for inverted pendulum: A comparative analysis of linear, nonlinear, and artificial intelligence approaches. *PLoS One*, 19(3):e0298093, 2024. doi: 10.1371/journal.pone.0298093.

[34] T. Liu, K. Liu, W. Luo, J. Kou, H. Zhan, G. Yu, Q. Guo, and Y. Shi. Motion gait recognition of lower limb exoskeleton based on particle swarm optimization-based extreme learning machine algorithm. *Actuators*, 14(3):120, 2025. doi: 10.3390/act14030120.

[35] G.-B. Huang, Q.-Y. Zhu, and C.-K. Siew. Extreme learning machine: theory and applications. *Neurocomputing*, 70(1–3):489–501, 2006. doi: 10.1016/j.neucom.2005.12.126.

[36] M. Ye, H. Wang, Z. Cao, J. Zheng, Z. Man, and X. Jin. Extreme-learning-machine-based robust AITSM control for steer-by-wire systems. In *2019 Chinese Control Conference (CCC)*, pages 2629–2634. IEEE, 2019. doi: 10.23919/ChiCC.2019.8865823.

[37] R. Chuei and Z. Cao. Extreme learning machine-based super-twisting repetitive control for aperiodic disturbance, parameter uncertainty, friction, and backlash compensations of a brushless DC servo motor. *Neural Computing and Applications*, 32:14483–14495, 2020. doi: 10.1007/s00521-020-04965-w.

[38] A.I. Roose, S. Yahya, and H. Al-Rizzo. Fuzzy-logic control of an inverted pendulum on a cart. *Computers & Electrical Engineering*, 61:31–47, 2017. doi: 10.1016/j.compeleceng.2017.05.016.

[39] Ü Önen. Model-free controller design for nonlinear underactuated systems with uncertainties and disturbances by using extended state observer based chattering-free sliding mode control. *IEEE Access*, 11:2875–2885, 2023. doi: 10.1109/ACCESS.2023.3234864.

[40] H. Gao, W. Tang, and R. Fu. Sliding mode control for hypersonic vehicle based on extreme learning machine neural network disturbance observer. *IEEE Access*, 10:69333–69345, 2022. doi: 10.1109/ACCESS.2022.3185256.